materials

MDPI

Article

Effects of Feed per Tooth and Radial Depth of Cut on Amplitude Parameters and Power Spectral Density of a Machined Surface

Qing Zhang [1,2] and Song Zhang [1,2,*]

[1] Key Laboratory of High Efficiency and Clean Mechanical Manufacture of MOE, School of Mechanical Engineering, Shandong University, Jinan 250061, China; zhangqing302@163.com

[2] Key National Demonstration Center for Experimental Mechanical Engineering Education, Shandong University, Jinan 250061, China

* Correspondence: zhangsong@sdu.edu.cn

Received: 19 February 2020; Accepted: 12 March 2020; Published: 14 March 2020

Abstract: Surface topography and roughness significantly affect the functional properties of engineering parts. In this study, a mathematical model simulating the surface topography in end milling is presented and verified by milling experiments. The three dimensional (3D) surface amplitude parameters (arithmetic average deviation S_{ba} and root mean square deviation S_q) of the milled surface were calculated by using the model and the effects of the product (p) and ratio (r) of radial depth of cut a_e and feed per tooth f_z on amplitude parameters were researched. To evaluate the lateral characteristics of the milled surface, one dimensional (1D) power spectral densities (PSD) along both feed and step-over direction were calculated and investigated. It was found that f_z affects 1D PSD along both directions, whereas a_e affects 1D PSD along the step-over direction. An angular spectrum, derived from the area power spectral density (APSD), was employed to research the spatial distribution of spectral energy on the milled surface. Furthermore, the influences of p and r on the PSD properties were researched. It was found that r is the significant factor that influences the direction of surface energy spectrum distribution.

Keywords: surface roughness; power spectral density; feed per tooth; radial depth of cut

1. Introduction

Surface roughness parameters that evaluate a machined surface can be classified into five categories: amplitude parameters, frequency parameters, hybrid parameters, functions and related parameters among others [1]. In the die casting process, friction is inevitable and surface topography of the dies significantly affects the interface friction behavior [2]. Root mean square (RMS) deviation of surface (S_q), density of summits (S_{ds}), and texture direction (S_{td}) have been accounted to influence the frictional property of the surfaces [3]. Among which, S_{td} is quantified by the angular spectrum of the surface which is derived from the area power spectral density (APSD). Besides, fatigue is another main failure mode of dies. The amplitude parameters of the machined surface have been proved to significantly affect the fatigue life of dies [4,5]. However, it has been suggested that S_{td} has also a significant effect on fatigue strength [6]. In consequence, the amplitude parameters and power spectral density (PSD) have significant influences on the friction property and fatigue performance of dies. Therefore, it becomes an important factor for improving the service life of dies to investigate and control the factors that affect machined amplitude parameters and PSD.

The amplitude parameters describe the ups and downs of the machined surface profile among which arithmetic average deviation S_{ba}, root mean square deviation S_q, and 10-point surface height S_z are most frequently used. In order to control the amplitude parameters, investigations on the effects of

tool eccentricity and helix angle [7], tool run-out and deflection [8], cutter path [9], tool inclination [10], machining and cooling method [11,12], material hardness [13], and cutting parameters [14–16] on surface roughness have been conducted. Cutting parameters play an important role among the factors that affect surface roughness since they affect both the surface roughness and the machining efficiency which can be estimated by the material removal rate (MRR). According to Zhang et al. [17], MRR shows increasing tendency when the product (p) of radial depth of cut (a_e) and feed per tooth (f_z) increases. However, different combinations of f_z and a_e cause different surface topographies with a determined value of p. Therefore, in this paper, the ratio (r) of f_z and a_e is introduced to calculate the value of f_z and a_e when p is determined.

The amplitude parameters contain the information that is perpendicular to the machined surface, whereas the lateral information cannot be presented. In order to obtain the lateral and frequency domain properties of a machined surface, PSD has been used to analyze surface topography. The method is based on Fourier Transformation which treats signals as a combination of sinusoidal harmonics with different phases, amplitudes, and frequencies. PSD was first employed to specify the surface topography of optical surfaces [18,19]. It has now been gradually applied to the characterization and analysis of surface topography. Michalski [20] found it useful to use an angular diagram and contour map of PSD for texture direction estimation of gear teeth flank surface topography. Jacobs et al. [21] presented three important drawbacks that impede the application of PSD to the functional characterization of surface topography and proposed strategies to mitigate them. Krolczyk et al. [22] studied the effect of feed value, cutting tool vibration, and cutting tool wear on the surface texture of duplex stainless steel using power spectral analysis. The wavelengths were also compared for dry and minimal quantity cooling lubrication (MQCL) machining. Kubiak et al. [23] investigated the effect of initial roughness on the surface during friction and wear processes. It was found that PSD can be used for quantitative determination of process versus frequency. Mishra et al. [24] comprehensively analyzed the roughness characterization of the machined surface at different tool overhangs. Khana et al. [25] researched the effects of feed and vibrations on surface roughness with the use of power spectral analysis. Duparre et al. [26] compared the surface roughness measured with six different instruments and measurement techniques by using the RMS roughness which was calculated from APSD functions. Peng and Kirk [27] compared the fast Fourier transform (FFT) plots and angular spectrum of different types of wear particles. It was demonstrated that the angular spectrum which is calculated from APSD can be used to study the angular position of the surface profile to the measurement coordinate. Dong and Stout [28] comprehensively described the procedure of implementing APSD with a two-dimensional FFT algorithm and presented some sampling considerations to obtain proper APSDs. Wu et al. [29] applied Fourier transforms and power spectral analysis to the characterization of articular cartilage surface. Angular spectrum was also employed to judge the isotropy and anisotropy of the surface. Cheung and Lee [30] employed the power spectral method to analyze surface roughness profiles in single-point diamond turning. They also researched the effect of feed rate, corner radius, vibration, tool interference, and material swelling on the power spectrum.

A mass of researches on the relationship between cutting parameters and amplitude parameters of machined surface has been conducted. However, fewer researches on surface roughness and machining efficiency with respect to the relationship between f_z and a_e have been undertaken. Furthermore, PSD has been used to compare the properties of the surface generated with different machining methods, and to research the effect of cutting parameters and dynamic behavior during machining on the machined surface based on experiments. However, fewer studies have been conducted on the influence of the relationship between f_z and a_e on the PSD of machined surface. In this research, the evaluation of surface amplitude parameters and PSD was carried out based on a mathematical model of the end-milled surface topography. First, a mathematical model which can simulate surface topography in end milling was introduced and assessed by experiment. Second, the effects of p and r on amplitude parameters (S_{ba} and S_q) were investigated using the surface topography model. Third, the 1D PSD was calculated along both feed and step-over direction. The effect of p and r on the 1D PSD profile was

researched. Finally, the angular spectrum was employed to analyze the distribution of PSD in different spatial directions of the machined surface.

2. Simulation Model of 3D Surface in End Milling

The surface topography model used in this research is based on our previous work and detailed introduced by Wang et al. ([31]). The modelling objective of this research is a round indexable insert (RDHW 10T3MO-MD04, Seco Company, Fagersta, Sweden) whose diameter is 10 mm. When the insert is fixed on the cutting tool, the axial rake angle is 4°.

2.1. Modelling of Cutting Tool Insert Trajectory

In order to describe the relative trajectory between cutting tool and workpiece, the machining coordinate systems were established as shown in Figure 1.

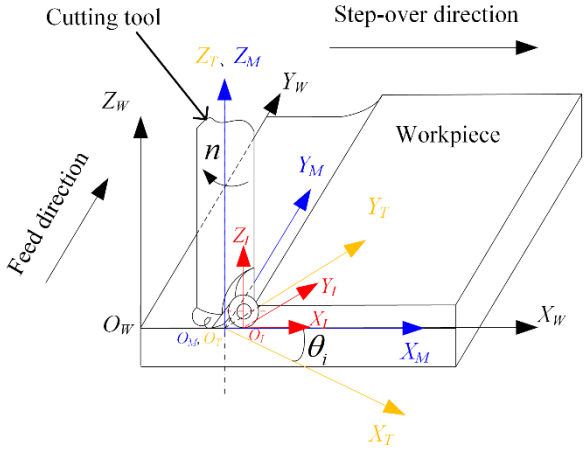

Figure 1. The machining coordinate systems used for the model.

The cutting insert coordinate system O_I-$X_IY_IZ_I$ is fixed on the cutting insert. The origin is the lowest point on the rake face. X_I axis is perpendicular to the cutting tool axis. Z_I axis is the ligature of the origin and the center of rake face and the positive direction of Z_I axis is upward.

The machine tool spindle coordinate system O_M-$X_MY_MZ_M$ is fixed on the cutting tool and moves together with the feed motion. The origin is on the axis of the cutting tool. The Y_M axis directs to the feed direction and the Z_M axis directs upward.

The cutting tool coordinate system O_T-$X_TY_TZ_T$ is on the cutting tool and rotates with the rotation of the spindle. The origin O_T coincides with O_M if no vibration occurs on the spindle. The X_T axis is parallel to the X_I axis and the Z_T axis is along the axis of the cutting tool.

The workpiece coordinate system O_W-$X_WY_WZ_W$ is set on the original machining point of the workpiece. The X_WY_W plane is parallel to the work surface to be processed. The X_W axis is along the step-over direction and Y_W is along the feed direction.

After the machining coordinate systems were established, the motion trajectory of the arbitrary point Q on the cutting edge was derived by coordinate transformations in sequence as O_I-$X_IY_IZ_I$ to O_T-$X_TY_TZ_T$, O_T-$X_TY_TZ_T$ to O_M-$X_MY_MZ_M$, O_M-$X_MY_MZ_M$ to O_W-$X_WY_WZ_W$. The kinematic equation of the cutting edge is as follows:

$$\begin{cases} x_W = R(1+\sin\alpha)\cos(\varphi_{i,1}+\omega t) + R(1-\cos\alpha)\sin(4^\circ)\sin(\varphi_{i,1}+\omega t) + (i-1)a_e \\ y_W = -R(1+\sin\alpha)\sin(\varphi_{i,1}+\omega t) + R(1-\cos\alpha)\sin(4^\circ)\cos(\varphi_{i,1}+\omega t) + v_f t \\ z_W = R(1-\cos\alpha)\cos(4^\circ) \end{cases} \quad (1)$$

where R is the radius of the cutting insert, α is the angle between the Z_I axis and the ligature between Q and the center of the rake face, ω is the angular speed of the cutting tool, i is the number of feed motion,

t is the cutting time from the beginning of the i_{th} feed motion until now, $\varphi_{i,1}$ is the initial cutting angle, a_e is the radial depth of cut, and v_f is the feed speed.

After the kinematic equation of the cutting edge was derived, the algorithm presented by Wang et al. ([31]) was used to generate the surface topography in end milling. The whole algorithm was realized by using MATLAB software (MATLAB 7.13, MathWorks, Natick, MA, USA).

2.2. Experimental Verification of the Model

A validating experiment was conducted to assess the simulation model. The cutting conditions employed in the experiment are shown in Table 1. The axial depth of cut a_p, cutting speed v_c, f_z and a_e, were introduced as design variables. The experiment was conducted on AISI H13 steel whose hardness is 50 ± 1 HRC after hardening and high temperature tempering heat treatment.

Table 1. Cutting conditions of the experiment.

No.	v_c (m/min)	f_z (mm/tooth)	a_e (mm)	a_p (mm)
1	250	0.3	1.8	0.2
2	190	0.25	1.8	0.5
3	220	0.35	0.6	0.8
4	160	0.35	1.2	1.4

A numerical control vertical machining center (YCM-V116B, Yongjin Machinery Co. LTD., Taiwan, China) was used to carry out the experiments. The maximum spindle speed of the machining center was 6000 r/min. One insert was employed and for every trial, a new insert was used to minimize the effect of tool wear. Dry machining and climb milling method were adopted.

The machined surfaces were observed by a white light interferometer (WYKO NT9300, Veeco Instruments Inc., Plainview, NY, USA). 3D arithmetic average deviation S_{ba} and 3D root mean square deviation S_q were employed so that the effect of the anisotropy characteristic of the milling surface could be taken into account. S_{ba} and S_q can be calculated as follows.

$$S_{ba} = \frac{1}{MN}\sum_{i=1}^{M}\sum_{j=1}^{N}\left|Z_{ij}\right| \tag{2}$$

$$S_q = \sqrt{\frac{1}{MN}\sum_{i=1}^{M}\sum_{j=1}^{N}\left(Z_{ij}\right)^2} \tag{3}$$

where M and N are the sampled data number in the sampling area along the feed and step-over directions, respectively. Z is the distance from the sampling points to the mean plane.

The comparison of 3D surface topography between simulation and experiment is shown in Figure 2. The comparison result indicates that the experimental and simulated surface topography show great consistency.

The simulated and experimental results are listed in Table 2, which shows that the relative error ranges of S_{ba} and S_q between simulation and experiment are 3.23%~12.99% and 2.75%~6.56%, respectively. In other word, the simulation model was efficient enough to predict the surface roughness for the cutting condition in this research.

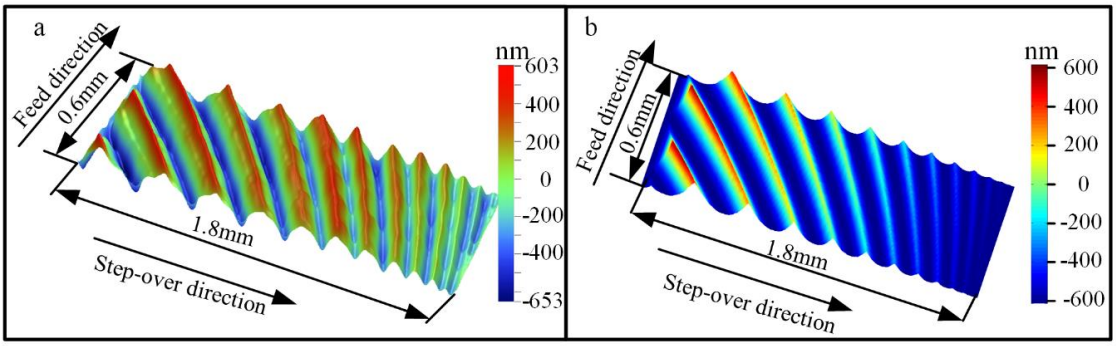

Figure 2. Comparison of surface topography (v_c = 250 m/min, f_z = 0.3 mm/z, a_e = 1.8 mm, a_p = 0.2 mm): (**a**) Experimental result; (**b**) simulated result.

Table 2. Results of the validation experiment.

No.	Surface Roughness	Experimental Result (μm)	Simulated Result (μm)	Error (%) [1]
1	S_{ba}	0.215	0.194	9.77
	S_q	0.255	0.248	2.75
2	S_{ba}	0.154	0.134	12.99
	S_q	0.183	0.171	6.56
3	S_{ba}	0.101	0.0904	10.5
	S_q	0.124	0.116	6.45
4	S_{ba}	0.186	0.180	3.23
	S_q	0.240	0.231	3.75

[1] Error = (Experimental result – Simulation result)/Experimental result.

3. Results and Discussion

3.1. Influence of p and r on Amplitude Parameters

To research the influence of p and r on amplitude parameters, the developed model in Section 2 was used to conduct a simulating trial. The design of the trial is shown in Table 3.

Table 3. S_{ba} (μm) for different values of p (mm^2/tooth) and r (/tooth).

r \ p	0.5	0.6	0.7	0.8	0.9	1
0.1	0.127	0.165	0.205	0.247	0.291	0.337
0.2	0.194	0.253	0.314	0.38	0.449	0.521
0.3	0.237	0.307	0.389	0.465	0.551	0.647
0.4	0.273	0.353	0.44	0.537	0.64	0.739
0.5	0.304	0.392	0.51	0.588	0.719	0.814
0.6	0.338	0.434	0.538	0.643	0.791	0.879

The simulation results are shown in Tables 3 and 4. The influence of r and p on the amplitude parameters (S_{ba} and S_q) is shown in Figure 3. Different to the research result of the ball-end milling condition [17], which illustrates that the profile of amplitude parameters versus r is like a 'check function', the surface roughness monotonously increases with the increase of r and p for the machining condition in this research.

Table 4. S_q (μm) for different values of p (mm^2/tooth) and r (/tooth).

r \ p	0.5	0.6	0.7	0.8	0.9	1
0.1	0.162	0.21	0.26	0.314	0.369	0.426
0.2	0.248	0.322	0.4	0.483	0.571	0.662
0.3	0.303	0.393	0.496	0.594	0.702	0.823
0.4	0.349	0.452	0.562	0.687	0.815	0.942
0.5	0.389	0.502	0.653	0.752	0.917	1
0.6	0.432	0.553	0.687	0.82	1	1.1

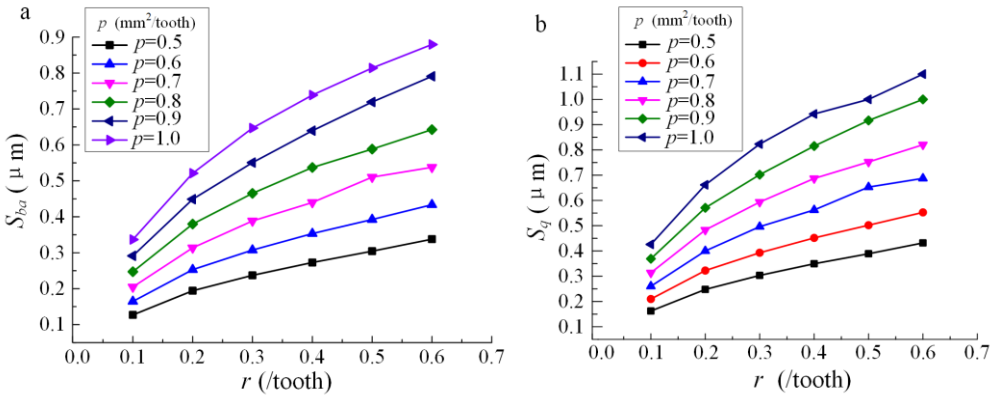

Figure 3. Profile of surface roughness under different p and r: (**a**) Profile of S_{ba}; (**b**) profile of S_q.

According to Figure 3, the profiles of S_{ba} and S_q versus r and p are similar to the exponential function. The function of surface roughness versus r and p can be expressed as:

$$S = Ar^B p^C \tag{4}$$

where S is the surface roughness, A is the constant coefficient of the exponential function. B and C are the exponential coefficients of the variables r and p, respectively.

Regression analysis was carried out by using the data in Tables 3 and 4 for S_{ba} and S_q, respectively. The regression model of S_{ba} and S_q can be expressed as follows.

$$S_{ba} = 1.202r^{0.523}p^{1.46} \tag{5}$$

$$S_q = 1.523r^{0.538}p^{1.41} \tag{6}$$

Analysis of Variance (ANOVA) was employed to carry out the significance test for the regression models. The results of ANOVA are shown in Tables 5 and 6. The value of P for the model is far less than 0.05. Thus, the relationships between amplitude parameters and the variables (p and r) are significant, in other word, the model is highly significant.

Table 5. ANOVA of the regression model for S_{ba}.

Model	Degree of Freedom	Sum of Squares	Mean Square	*F* Value	*P*
Regression	2	7.8912	3.9456	7201.76	0.000
Residual	33	0.0181	0.0005		
Total	35	7.9092	R^2: 0.998, R^2(*Adj.*): 0.998		

Table 6. ANOVA of the regression model for S_q.

Model	Degree of Freedom	Sum of Squares	Mean Square	*F* Value	*P*
Regression	2	7.8022	3.9011	5719.82	0.000
Residual	33	0.0225	0.0007		
Total	35	7.8247	R^2: 0.997, $R^2(Adj.)$: 0.997		

3.2. Research on PSD Based on the Simulation Model

The 3D surface evaluation parameters (S_{ba} and S_q) researched in Section 3.1 can be used to evaluate the characteristic of the machined surface along the normal direction of the machined surface. However, the lateral information of the machined surface cannot be analyzed. In addition, the anisotropy of the milled surface is also neglected in the amplitude parameters. So, in order to comprehensively analyze the milled surface topography, PSD was employed to describe the spatial frequency spectrum of the machined surface.

3.2.1. PSD of the Machined Surface

1D PSD is used to analyze the frequency-domain characteristics of a surface profile along a specified direction (e.g., feed and step-over direction). The definition of the 1D PSD for a continuous surface profile $z(x)$ is represented as follows:

$$Z(f_x) = \lim_{T_x \to \infty} \frac{1}{T_x} \left| \int_{-\infty}^{\infty} z(x) \exp(-j2\pi x f_x) dx \right|^2 \tag{7}$$

where $Z(f_x)$ is the PSD of $z(x)$, f_x is the frequency, and T_x is the length of the surface profile.

In practice, the machined surface is usually obtained by a digitizing method with equal sampling intervals $\triangle x$ and fixed number (N_x) of sampling points. So, PSD should be transformed into a discrete form as follows:

$$Z(f_p) = \frac{\Delta x}{N_x} \left| \sum_{k=0}^{N_x-1} z(x_k) \exp(-j2\pi pk/N_x) \right|^2 \tag{8}$$

where $p = 0, 1, 2, \ldots, N_x - 1, f_p = p/(N_x \triangle x)$.

The research of 1D PSD depends on the direction of analysis, however, in order to research the whole frequency information of a 3D machined surface, APSD should be employed. Analogously to the derivation of 1D PSD, the APSD of a machined surface can be evaluated as follows:

$$Z(f_p, f_q) = \frac{\Delta x \Delta y}{N_x N_y} \left| \sum_{l=1}^{N_x-1} \sum_{k=1}^{N_y-1} z(x_k, y_l) \exp[-j2\pi(pk/N_x + ql/N_y)] \right|^2 \tag{9}$$

where N_x and N_y are the sampled data numbers along x and y direction, respectively, $p = 0, 1, 2, \ldots, N_x - 1, q = 0, 1, 2, \ldots, N_y - 1$, $\triangle x$ and $\triangle y$ are the sampling interval along the x and y direction, $f_p = p/(N_x \triangle x), f_q = q/(N_y \triangle y)$.

In addition, the angular spectrum which can be used to research the distribution of APSD in different spatial directions was also employed. For the calculation of the angular spectrum, APSD $Z(f_p f_q)$ in the Cartesian coordinate is first transferred into $Z(f_r, \theta)$ in the polar coordinate, and then the angular spectrum can be calculated as follows.

$$S(\theta) = \int_0^{\frac{1}{2\sqrt{(\Delta x \cos\theta)^2 + (\Delta y \sin\theta)^2}}} Z(f_r, \theta) df_r \quad 0^\circ \le \theta \le 179^\circ \tag{10}$$

3.2.2. Influence of p and r on 1D PSD

In order to research the influence of p and r on 1D PSD, the developed model in Section 2 was used to conduct a simulating trial. The design of the trial is shown in Table 7. The surface profiles along feed direction (Y direction) and step-over direction (X direction) were extracted from the simulated surface topography and used to analyze the PSD. For each direction, 40 profiles at different locations were extracted. Then the average of the calculated PSD was used for the final result.

Table 7. Design of the simulating trials (v_c = 250 m/min, a_p = 0.2 mm).

No.	1	2	3	4	5	6	7	8	9	10	11
r (/tooth)	0.1	0.2	0.3	0.4	0.5	0.6	0.1	0.1	0.1	0.1	0.1
p (mm^2/tooth)	0.5	0.5	0.5	0.5	0.5	0.5	0.6	0.7	0.8	0.9	1

The effect of p and r on the 1D PSD profile is shown in Figure 4. It can be seen that PSD is concentrated in several ranges of frequencies. For the PSD profile along the step-over direction, there exist two peaks, whereas only one obvious peak is found for that along the feed direction. Figure 4 also describes that the PSD amplitude is higher with higher values of both p and r along the feed and step-over directions. This complies with the conclusion in Section 3.1 that the amplitude parameters monotonously increases with the increase of r and p.

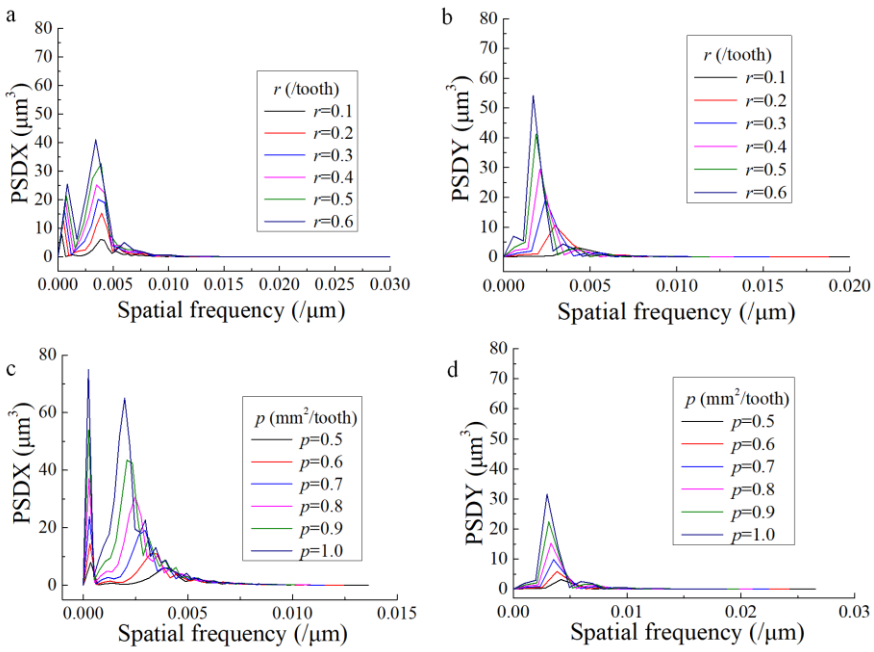

Figure 4. Effects of r and p on 1D power spectral density (PSD) along different directions (**a**) Effect of r on 1D PSD along step-over direction; (**b**) Effect of r on 1D PSD along feed direction; (**c**) Effect of p on 1D PSD along step-over direction; (**d**) Effect of p on 1D PSD along feed direction.

The frequencies corresponding to the peaks of the PSD profiles were extracted and the wavelengths corresponding to these frequencies are shown in Table 8, in which X_{p1} and X_{p2} are the wavelengths for the first and second peaks of the PSD profile along the step-over direction, Y_p is the wavelength for the peak of the PSD profile along the feed direction.

Table 8. Wavelength corresponding to the peaks of the power spectral density (PSD) profile (v_c = 250 m/min, a_p = 0.2 mm).

No.	R (/tooth)	P (mm^2/tooth)	f_z (mm/tooth)	a_e (mm)	X_{p1} (mm)	X_{p2} (mm)	Y_p (mm)
1	0.1	0.5	0.224	2.236	2.862	0.26	0.239
2	0.2	0.5	0.316	1.581	2.024	0.253	0.337
3	0.3	0.5	0.387	1.291	1.653	0.275	0.413
4	0.4	0.5	0.447	1.118	1.431	0.286	0.477
5	0.5	0.5	0.500	1.000	1.28	0.256	0.533
6	0.6	0.5	0.548	0.913	1.169	0.292	0.584
7	0.1	0.6	0.245	2.449	3.135	0.285	0.261
8	0.1	0.7	0.265	2.646	3.387	0.339	0.282
9	0.1	0.8	0.283	2.828	3.62	0.402	0.302
10	0.1	0.9	0.300	3.000	3.84	0.48	0.32
11	0.1	1	0.316	3.162	4.048	0.506	0.337

It can be found from Table 8 that X_{p1} values for all the trials are approximately 1.28 times of the values of a_e which means that the effect of a_e on the surface profile along the step-over direction is significant. In addition, Y_p values for all the trials are approximately 1.07 times of the values of f_z which means f_z is the most significant factor that influences the surface contour along the feed direction. Furthermore, it is interesting that the value of X_{p2} barely changes with the increase of r whereas it shows an increasing tendency when p increases. Obviously, when the value of p is constant, f_z increases and a_e decreases with the increase of r. This may be the reason why the value of X_{p2} remains quasi-constant with the increase of r. In another words, the second peak of the PSD profile along the step-over direction is the result of the common influence of f_z and a_e.

3.2.3. Research on APSD and the Angular Spectrum of the Milled Surface

The APSD and angular spectrum of all the trials in Table 7 were calculated and the results of two example trials are presented in Figure 5. It can be seen from the APSD that the amplitudes concentrate at several prominent frequencies and the surface texture distributes along specific directions. The angular spectrum can indicate the angle position of spectral intensity to the X axis in the X–Y plane. The angular spectrum profile in "Figure 5c,f" shows several peaks at the corresponding angles. It can be found that the number of the angle spectrum peaks for the specific machined surface approximately equals the number of residual ridges on the surface topography in "Figure 5a,d". This is because the contour map of APSD is perpendicular to the surface texture direction [20]. So, for every ridge of the machined surface, a spectral energy distribution exists along the direction perpendicular to the ridge orientation.

Furthermore, it also can be seen from Figure 5c,f that for each angular spectrum, there exists a maximum peak. The effect of p and r on the maximum peak amplitude and the corresponding angle is shown in Figure 6. The result shows that the maximum amplitude of the energy spectrum has a tendency to increase when r increases, while the corresponding angle tends to decrease. With the increase of p value, the maximum amplitude of the energy spectrum tends to increase, while the corresponding angle barely changes. In other words, the effect of p on the distribution direction of the surface energy spectrum is not significant. The main factor influencing the direction of surface energy spectrum distribution is the value of r.

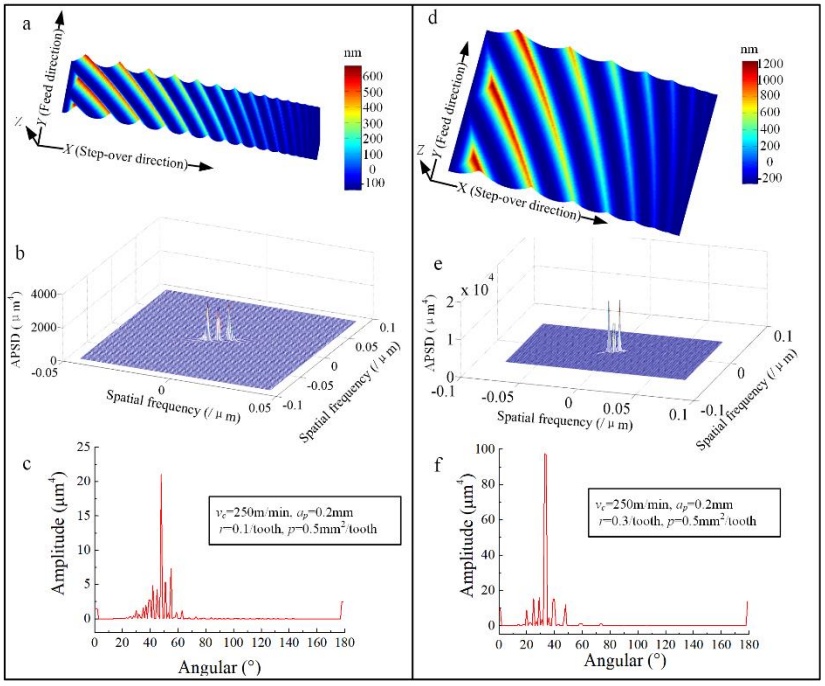

Figure 5. Three-dimensional surface topography and its area power spectral density (APSD) and angular spectrum. (**a**,**d**) Three dimensional surface topography; (**b**,**e**) APSD of the surface; (**c**,**f**) Angular spectrum.

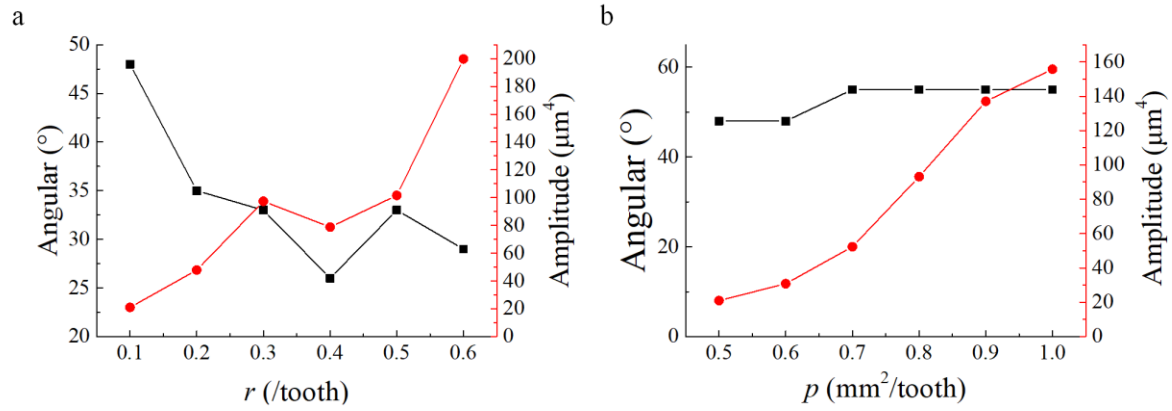

Figure 6. Effect of p and r on the peak amplitudes of the angular spectrum and the corresponding angular. (**a**) Effect of r; (**b**) Effect of p.

4. Conclusions

Based on a surface topography model, the amplitude surface roughness (S_{ba} and S_q) and PSD of the end milled surface were calculated. The effects of p and r on S_{ba}, S_q and PSD were also investigated. The conclusions derived from the research can be summarized as follows:

- S_{ba} and S_q have a monotonous tendency to increase with the increase of r and p. The exponential models of S_{ba} and S_q versus r and p were fitted.
- The effects of p and r on the 1D PSD profile along the feed direction and step-over direction were researched. The result shows that the PSD amplitude is higher with higher values of both p and r along the feed and step-over directions. f_z affects the peaks of the 1D PSD along both directions whereas a_e affects the peak of the 1D PSD along the step-over direction.

- The angular spectrum of the surface was calculated by the APSD. It can be found that the number of the angle spectrum peaks for the specific machined surface approximately equals the number of residual ridges on the surface topography. The research on the effect of p and r on the angular spectrum reveals that r is the dominant factor influencing the direction of surface energy spectrum distribution.

Author Contributions: Conceptualization, Q.Z. and S.Z.; methodology, Q.Z. and S.Z.; software, Q.Z. and S.Z.; validation, Q.Z. and S.Z.; formal analysis, Q.Z. and S.Z.; investigation, Q.Z. and S.Z.; resources, Q.Z. and S.Z.; data curation, Q.Z. and S.Z.; writing—original draft preparation, Q.Z. and S.Z.; writing—review and editing, Q.Z. and S.Z.; visualization, Q.Z. and S.Z.; supervision, S.Z.; project administration, S.Z.; funding acquisition, S.Z. All authors have read and agreed to the published version of the manuscript.

Funding: This work was supported by the National Natural Science Foundation of China (Grants No. 51975333 and No. 51575321), the Key Research & Development Program (Major Science and Technology Innovation Project) of Shandong Province (Grant No. 2019JZZY010437), and Taishan Scholar Project of Shandong Province (No. ts201712002).

Acknowledgments: The authors highly appreciate their colleagues at Shandong University for conducting the experiments. Furthermore, the authors would like to thank the reviewers for their valuable comments and editors for improving the manuscript.

Conflicts of Interest: The authors declare no conflict of interest.

References

1. Krolczyk, G.M.; Maruda, R.W.; Krolczyk, J.B.; Nieslony, P.; Wojciechowski, S.; Legutko, S. Parametric and nonparametric description of the surface topography in the dry and MQCL cutting conditions. *Measurement* **2018**, *121*, 225–239. [CrossRef]
2. Menezes, P.L.; Kishore; Kailas, S.V. Effect of surface roughness parameters and surface texture on friction and transfer layer formation in tin–steel tribo-system. *J. Mater. Process. Technol.* **2008**, *208*, 372–382. [CrossRef]
3. Singh, R.; Melkote, S.N.; Hashimoto, F. Frictional response of precision finished surfaces in pure sliding. *Wear* **2005**, *258*, 1500–1509. [CrossRef]
4. Suraratchai, M.; Limido, J.; Mabru, C.; Chieragatti, R. Modelling the influence of machined surface roughness on the fatigue life of aluminium alloy. *Int. J. Fatigue* **2008**, *30*, 2119–2126. [CrossRef]
5. Guillemot, N.; Lartigue, C.; Billardon, R.; Mawussi, B.K. Prediction of the endurance limit taking account of the microgeometry after finishing milling. *IJIDeM* **2010**, *4*, 239–249. [CrossRef]
6. Novovic, D.; Dewes, R.C.; Aspinwall, D.K.; Voice, W.; Bowen, P. The effect of machined topography and integrity on fatigue life. *Int. J. Mach. Tools Manuf.* **2004**, *44*, 125–134. [CrossRef]
7. Buj-Corral, I.; Vivancos-Calvet, J.; González-Rojas, H. Influence of feed, eccentricity and helix angle on topography obtained in side milling processes. *Int. J. Mach. Tools Manuf.* **2011**, *51*, 889–897. [CrossRef]
8. Ryu, S.H.; Choi, D.K.; Chu, C.N. Roughness and texture generation on end milled surfaces. *Int. J. Mach. Tools Manuf.* **2006**, *46*, 404–412. [CrossRef]
9. Shaghayegh, S.; Hossein, S.M.; Hamed, H. The influence of tool path strategies on cutting force and surface texture during ball end milling of low curvature convex surfaces. *Sci. World J.* **2014**, *2014*, 1–14.
10. Lavernhe, S.; Quinsat, Y.; Lartigue, C. Model for the prediction of 3D surface topography in 5-axis milling. *Int. J. Adv. Manuf. Technol.* **2010**, *51*, 915–924. [CrossRef]
11. Chen, X.; Zhao, J.; Zhang, W. Influence of milling modes and tool postures on the milled surface for multi-axis finish ball-end milling. *Int. J. Adv. Manuf. Technol.* **2015**, *77*, 2035–2050. [CrossRef]
12. Mia, M.; Dhar, N.R. Prediction of surface roughness in hard turning under high pressure coolant using Artificial Neural Network. *Measurement* **2016**, *92*, 464–474. [CrossRef]
13. Mia, M.; Dhar, N.R. Modeling of Surface Roughness Using RSM, FL and SA in Dry Hard Turning. *Arab. J. Sci. Eng.* **2018**, *43*, 1125–1136. [CrossRef]
14. Yang, D.; Liu, Z. Surface topography analysis and cutting parameters optimization for peripheral milling titanium alloy Ti–6Al–4V. *Int. J. Refract. Met. Hard Mater.* **2015**, *51*, 192–200. [CrossRef]
15. Tangjitsitcharoen, S.; Thesniyom, P.; Ratanakuakangwan, S. Prediction of surface roughness in ball-end milling process by utilizing dynamic cutting force ratio. *J. Intell. Manuf.* **2017**, *28*, 13–21. [CrossRef]

16. Twardowski, P.; Wojciechowski, S.; Wieczorowski, M.; Mathia, T. Surface roughness analysis of hardened steel after high-speed milling. *Scanning* **2011**, *33*, 386–395. [CrossRef]
17. Zhang, Q.; Zhang, S.; Shi, W. Modeling of surface topography based on relationship between feed per tooth and radial depth of cut in ball-end milling of AISI H13 steel. *Int. J. Adv. Manuf. Technol.* **2018**, *95*, 4199–4209. [CrossRef]
18. Lawson, J.K.; Wolfe, C.R.; Manes, K.R.; Trertholme, J.B.; Aikens, D.M.; English, R.E., Jr. Specification of optical components using the power spectral density function. *Proc. SPIE 2536, Opt. Manuf. Test.* **1995**, *2536*, 38–50.
19. Alcock, S.G.; Ludbrook, G.D.; Owen, T.; Dockree, R. Using the power spectral density method to characterise the surface topography of optical surfaces. *Proc. SPIE 7801, Adv. Metrol. X-Ray EUV Opt. III* **2010**, *7801*, 1–8.
20. Michalski, J. Surface topography of the cylindrical gear tooth flanks after machining. *Int. J. Adv. Manuf. Technol.* **2009**, *43*, 513–528. [CrossRef]
21. Jacobs, T.D.B.; Junge, T.; Pastewka, L. Quantitative characterization of surface topography using spectral analysis. *Surf. Topogr. Metrol. Prop.* **2017**, *5*, 013001. [CrossRef]
22. Krolczyk, G.M.; Maruda, R.W.; Nieslony, P.; Wieczorowski, M. Surface morphology analysis of duplex stainless steel (DSS) in clean production using the power spectral density. *Measurement* **2016**, *94*, 464–470. [CrossRef]
23. Kubiak, K.J.; Bigerelle, M.; Mathia, T.G.; Dubois, A.; Dubar, L. Dynamic evolution of interface roughness during friction and wear processes. *Scanning* **2014**, *36*, 30–38. [CrossRef] [PubMed]
24. Mishra, V.; Khan, G.S.; Chattopadhyay, K.D.; Nand, K.; Sarepaka, R.G.V. Effects of tool overhang on selection of machining parameters and surface finish during diamond turning. *Measurement* **2014**, *55*, 353–361. [CrossRef]
25. Khan, G.S.; Sarepaka, R.G.V.; Chattopadhyay, K.D.; Jain, P.K.; Bajpai, R.P. Characterization of nanoscale roughness in single point diamond turned optical surfaces using power spectral density analysis. *Indian J. Eng. Mater. Sci.* **2004**, *11*, 25–30.
26. Duparré, A.; Ferre-Borrull, J.; Gliech, S.; Notni, G.; Steinert, J.; Bennett, J.M. Surface Characterization Techniques for Determining the Root-Mean-Square Roughness and Power Spectral Densities of Optical Components. *Appl. Opt.* **2002**, *41*, 154–41171. [CrossRef] [PubMed]
27. Peng, Z.; Kirk, T.B. Two-dimensional fast Fourier transform and power spectrum for wear particle analysis. *Tribol. Int.* **1997**, *30*, 583–590. [CrossRef]
28. Dong, W.P.; Stout, K.J. Two-dimensional fast Fourier transform and power spectrum for surface roughness in three dimensions. *Proc. Inst. Mech. Eng., Part. B* **1995**, *209*, 381–391. [CrossRef]
29. Wu, J.P.; Kirk, T.B.; Peng, Z.; Miller, K.; Zheng, M.H. Utilization of two-dimensional fast Fourier transform and power spectral analysis for assessment of early degeneration of articular cartilage. *J. Musculoskelet. Res.* **2005**, *9*, 119–131. [CrossRef]
30. Cheung, C.F.; Lee, W.B. Characterisation of nanosurface generation in single-point diamond turning. *Int. J. Mach. Tools Manuf.* **2001**, *41*, 851–875. [CrossRef]
31. Wang, P.; Zhang, S.; Li, Z.; Li, J. Tool path planning and milling surface simulation for vehicle rear bumper mold. *Adv. Mech. Eng.* **2016**, *8*, 1–10. [CrossRef]